Classical trajectories on simple model potentials for N_2–Kr: Comparison with relaxation and other data

Marc A. ter Horst[a] and Cynthia J. Jameson
Department of Chemistry M/C-111, University of Illinois at Chicago, Chicago, Illinois 60607-7061

(Received 16 August 1994; accepted 8 December 1994)

We compare the ability of six N_2–Kr potential energy surfaces to predict experimental interaction second virial coefficients, diffusion coefficients, mixture viscosity, thermal conductivity, and nuclear magnetic resonance (NMR) rotational relaxation cross sections. These include a previously published empirical surface derived from fits to molecular beam experiments and various model potentials of the Tang and Toennies (TT) type. The TT type potentials differ in the set of dispersion coefficients employed. Two sets are obtained from published *ab initio* calculations, another from combining rules and one from empirical considerations. The repulsive parameters have been obtained from published results of a charge overlap combining rule. A variation of the TT model suggested by Aziz is also used to further investigate the effect of the repulsive wall anisotropy on the rotational relaxation cross sections. Forty-five effective cross sections that determine the bulk transport and relaxation phenomena have been calculated by classical trajectories for temperatures ranging from 100 to 800 K. The sensitivity of the NMR-derived cross sections to the various characteristics of the anisotropy of the potential (such as the anisotropy in the well depth, in the high repulsive wall, in the low repulsive wall, and at $V=0$) are examined. The empirical anisotropic LJ(12,6) surface of Rotzoll provides the best agreement with the diffusion, viscosity, thermal conductivity, and NMR relaxation experimental results.

I. INTRODUCTION

The potential energy surface for atom–diatomic interactions are of current interest. The H_2–rare gas potential energy surfaces have been extensively tested and are now considered well established.[1] These are weakly anisotropic systems so that essentially separate determinations of the isotropic and anisotropic parts of the potential can be achieved. The N_2–rare gas systems are much more challenging. Beneventi and McCourt and co-workers have used close-coupling methods and classical trajectory (CT) methods to test empirical surfaces and model surfaces for N_2–He and N_2–Ne.[2,3] They have developed an empirical potential energy surface (PES) for N_2–Ar based on extensive multiproperty fitting.[4] In the H_2–rare gas[5–8] and in N_2–Ar systems,[4] it has been established that nuclear spin relaxation data prove to be very useful in testing and refining the anisotropic part of the potential. In particular the H_2–He potential surface has been refined by making use of the ^{1}H and ^{2}D spin relaxation data for H_2–He, HD–He, and D_2–He.[5,6] The high sensitivity of the temperature dependence of the ^{1}H relaxation in the H_2–Ne system enabled a minor adjustment of the anisotropic part of a PES that had already reproduced rather well many observables, in order to fit the close-coupled scattering calculations of $(T_1/\rho)^{\infty}_{\text{lin}}$ to the observed data in the H_2–Ne mixtures.[7] A recently determined multiproperty PES for N_2–Ar was also refined by using nuclear spin relaxation times. This PES provides the best overall agreement with all available gas phase data for N_2–Ar mixtures.[4] The N_2–He, Ne, and Ar intermolecular interactions can now be considered well-characterized for predictions of scattering, transport, and relaxation data. We consider next the N_2–Kr and N_2–Xe systems.

A model potential that has been proposed for N_2–rare gas systems is that of Kistemaker and de Vries (KdV) which is based on a sum of two site-to-site Morse functions,[9] with parameters determined from combining rules[10] using the pure gas parameters.[11] A set of classical trajectories were run on such N_2–He, –Ne, –Ar, and –Xe surfaces to compare calculated rotational relaxation times (τ_{rot}) with experimental results.[9] The authors report good agreement between the PES predictions and experiment. On the other hand, in a sequence of studies on N_2–He, N_2–Ne, and N_2–Ar surfaces, Wong calculated a number of observables from the KdV surfaces including interaction second virial coefficients (B_{12}) and rotational relaxation times.[12] The ability of the KdV surfaces to reproduce experimental B_{12} values decreased in going from N_2–He to N_2–Ar and the values for τ_{rot} did not agree with experiment or the original calculated values. Since this latter CT approach has shown good agreement with the close-coupling method,[13] it was concluded that the KdV surface does not provide a sufficiently adequate description of the N_2–Ar interactions. The poor quality of the N_2–Ar KdV surface is probably due to the use of a simple combining rule and the neglect of a three body contribution. We could have used combining rules to construct a N_2–Kr surface of the same form as Kistemaker and de Vries constructed for N_2–He, Ne, Ar, and Xe. However, on the basis of its diminishing agreement with experiment in the series N_2–He, –Ne, –Ar, we do not consider the KdV potential any further for N_2–Kr.

Another model anisotropic potential for symmetric rigid rotor ($D_{\infty h}$ symmetry)-atom systems that has been proposed by Pack,[14] builds the anisotropy into the parameters for the

[a]Present address: Northwestern University, Evanston, Illinois 60208-3113.

well depth, ϵ, and its radial position, R_m. Pack has shown that both anisotropies could be determined from those molecular beam scattering experiments in which both the rainbow region and the diffraction oscillations are precisely determined. In particular, a Lennard-Jones (12,6) with a Legendre expansion [truncated at the $P_2(\cos\theta)$ term] in the well depth and its radial position is a simple form which could be used. Rotzoll[15] reported anisotropic potentials of this form for the N_2–Ar, Kr and O_2–Ar, Kr systems in which the parameters for the anisotropic Lennard-Jones [LJ(12,6)] functions were determined from fits to laboratory angular distributions obtained from molecular beam experiments. This appears to be the first anisotropic surface proposed for the N_2–Kr system.

Of the model surfaces that have been used for N_2–He, N_2–Ne, and N_2–Ar, the Bowers, Tang, and Toennies PES (Ref. 16) (called BTT) provides remarkably good descriptions of the intermolecular interaction for these pairs. In the Tang–Toennies model potential, the long range *ab initio* dispersion terms are damped individually using a universal damping function, and a simple Born–Mayer repulsive term is added to them.[17] When a large number of different experimental quantities are available for multiproperty fitting, a useful approach is to construct an empirical piecewise PES, for example a Morse–Morse–spline–van der Waals (MMSV) form. This approach has been used for N_2–Ne, and N_2–Ar.[2,4,18] In comparison, the BTT potential for each of these systems provides an adequate description; although it does not give as accurate a prediction of some data as the empirical surface, it does better than the empirical surface in others. For example it gives better agreement with the rotational relaxation and field effect data, which are properties sensitive to the anisotropy of the high repulsive wall for N_2–He while giving simultaneous agreement with the scattering data, the second virial coefficient data, the bulk transport data, and the depolarized Rayleigh collision-broadening data which are properties sensitive to the anisotropy of the low repulsive wall and the spherical component of the interaction.[3] For N_2–Ne the BTT potential gives impressive agreement with the experimental results over a wide temperature range for mixture transport phenomena and specially for rotational relaxation and field-effect data.[19] For N_2–Ar (Ref. 20) the BTT surface was the best available, until just recently,[4] reproducing transport properties such as diffusion and shear viscosity to within $\pm 1\%$ over the temperature range 120–1000 K and the thermal conductivity at room temperature. However, the properties which are highly sensitive to the anisotropy of the interaction, such as relaxation and field effect phenomena, are less well predicted. The most recent empirical surface that gives the best overall description of the N_2–Ar interaction[4] and the BTT surface have similar isotropic parts while the anisotropy in the empirical surface is not as strong as in the BTT version.

For the next member of the series, the N_2–Kr pair, there are not as many accurately measured observables as would be needed to construct a multiproperty potential. Nevertheless, there are second virial coefficients from 148 to 323 K by Brewer,[21] laboratory angular distributions from molecular beam scattering experiments,[22] diffusion coefficients,[23,24] mixture viscosity,[25] thermal conductivity,[26] and temperature-dependent NMR relaxation cross sections of two types (σ_J and $\sigma_{\theta,2}$) from our laboratory.[27,28] In T_1 studies of mixtures of N_2 with other gases we have discovered a very interesting experimental trend: the ratio $\sigma_{\theta,2}/\sigma_J$ for N_2 molecule is very nearly independent of the collision partner and is close to 2.1. These collision partners include a wide variety of molecular types, Ar, Kr, Xe, CO, N_2, HCl, CO_2, CH_4, CF_4, SF_6. In addition we have discovered some trends in the σ_J values that have been measured in our laboratory for a large number of probe molecules and these ten collision partners.[29] These two cross sections are known to be extremely sensitive to the anisotropy of the potential energy surface. Spin relaxation phenomena depend entirely on the anisotropy of the PES of the interaction between the colliding pair of molecules, as was recognized very early on by Bloom and others[30] and by Gordon.[31] From the work of McCourt and co-workers[4] we know that a multiproperty fitted PES can reproduce our measured $\sigma_J(T)$ and $\sigma_{\theta,2}(T)$ for the N_2–Ar system. Therefore, in our quest to understand the near-independence of the $\sigma_{\theta,2}/\sigma_J$ ratio with respect to the collision partner and the general empirical trends in the σ_J, we have some hope of a quantitative understanding of the trends in N_2–Ar, Kr, Xe. Toward this end, we begin with classical trajectory studies of the N_2–Kr system.

We considered the currently available potential function for N_2–Kr in the literature by Rotzoll[15] and we also constructed new potentials using the TT model. In their study of N_2–noble gas atom interactions, Bowers, Tang, and Toennies (BTT) (Ref. 16) use the Tang–Toennies (TT) model[17] to construct anisotropic surfaces for the N_2–He, –Ne, and –Ar systems. In the TT model, the PES is expanded in a Legendre series with each of the $V_n(R)$ a linear combination of cuts of the surface at various values for θ, where θ is the angle between the axis of the linear rotor and the line of centers. A Born–Mayer repulsive term and a damped dispersion series are used in each cut and *ab initio* values are used for the Born–Mayer parameters $A(\theta)$, $b(\theta)$, and also for the dispersion coefficients. Bowers *et al.* noted that for each of the interactions, plots of the cuts at $\theta=0°$ and $\theta=90°$ reduce to similar curves. The authors suggested that these reduced curves could be used to construct anisotropic N_2–Kr and N_2–Xe surfaces. We instead use the Born–Mayer parameters for the N_2–heavy noble gas systems that have been reported by Nyeland and Toennies.[32] A and b values for the parallel ($\theta=0°$) and perpendicular ($\theta=90°$) configurations were derived from charge-overlap integrals using a site-to-site description of the charge distribution. In combination with values for the dispersion coefficients, potential energy surfaces for the N_2–Kr and N_2–Xe systems can be constructed. This is the approach that we adopt. The success of the simple BTT model potential in describing the isotropic component of the PES in N_2–He, Ne, Ar provides some encouragement that the BTT recipe could be used for constructing model potentials for N_2–Kr and N_2–Xe. We consider only the N_2–Kr anisotropic potential surfaces in this paper.

In this paper we report classical trajectory calculations on the N_2–Kr system using several model potentials, and we compare their ability to predict our experimental NMR re-

laxation data and also other experiments such as second virial coefficients, diffusion coefficients, and mixture viscosity. We find that the anisotropic Lennard-Jones potential of Rotzoll does surprisingly well in providing good overall agreement with these properties and with $\sigma_J(T)$ and $\sigma_\theta(T)$ cross sections obtained from NMR spin relaxation measurements.

II. THE N_2–Kr POTENTIAL SURFACES

We use the previously published anisotropic N_2–Kr PES by Rotzoll and construct several model anisotropic surfaces of the TT type. The Rotzoll (GR) functional form follows the basic Lennard-Jones (12,6) function with the anisotropy written in the well depth and radial position

$$V(R,\theta)=\epsilon(\theta)\{[R_m(\theta)/R]^{12}-2[R_m(\theta)/R]^6\}$$

with

$$\epsilon(\theta)=\bar{\epsilon}[1+aP_2(\cos\ \theta)]$$

and

$$R_m(\theta)=\bar{R}_m[1+bP_2(\cos\ \theta)].$$

The values of the parameters determined by Rotzoll are

$$\bar{\epsilon}=2.25\times10^{-14}\ \text{erg}\quad a=-0.25$$

$$R_m=4.00\ \text{Å}\quad b=0.09.$$

We have assembled new anisotropic N_2–Kr surfaces using the Tang–Toennies model as had been done for the N_2–He, Ne, and Ar systems.[16] The general TT surface for a linear molecule–atom system is written as a Legendre expansion in cos θ, $V(R,\theta)=\Sigma_n V_n(R)P_n(\cos\theta)$.[17] Due to the symmetry of the N_2–rare gas atom systems, the odd terms are eliminated and only the zero and even order Legendre polynomials contribute. Retaining the first two terms one obtains

$$V(R,\theta)=V_0(R)+V_2(R)P_2(\cos\ \theta).$$

In this paper, the radial contributions are determined from linear combinations of cuts of the surface at θ=0° and 90°,

$$V_0(R)=[V(R,0°)+2V(R,90°)]/3,$$

$$V_2(R)=2[V(R,0°)-V(R,90°)]/3.$$

Following the TT recipe, each $V(R,\theta)$ is written as a combination of a Born–Mayer repulsive term, a damping function and a dispersion coefficient series,

$$V(R,\theta)=A(\theta)\exp[-b(\theta)R]-\sum_{n\geq3}^{n_{\max}}\left\{1-\sum_{k=0}^{2n}\frac{[b(\theta)R]^k}{k!}\times\exp[-b(\theta)R]\right\}\frac{C_{2n}(\theta)}{R^{2n}},$$

where

$$C_{2n}(\theta)=C_{2n}[1+\Gamma_{2n}^{(2)}P_2(\cos\ \theta)+\Gamma_{2n}^{(4)}P_4(\cos\ \theta)+\cdots].$$

The estimates of the Born–Mayer parameters for the N_2–heavy noble gas systems have been reported by Nyeland and Toennies[32] and are listed in Table I. In this site–site approximation,[32] the repulsive part of the potential is determined from charge density overlaps of the site-to-site charge distributions separately for the parallel and perpendicular geometries. This potential is then fitted to the Born–Mayer potential form

$$V_\parallel=A_\parallel\exp(-b_\parallel R_\parallel),\quad V_\perp=A_\perp\exp(-b_\perp R_\perp).$$

Nyeland and Toennies found that potentials V_{AB} are related to the overlap integrals of the undisturbed electron density distributions of atoms A and B by

$$V_{AB}=K_{AB}[S(\rho_A\rho_B)/R^2]^{\gamma_{AB}},$$

where the parameters K_{AB} and γ_{AB} may be obtained by geometric and arithmetic combining rules respectively when $A\neq B$. They obtained A and b parameters for parallel and perpendicular arrangements of the N_2 molecule and a rare gas atom.[32] The advantage of this model is that the method can easily be extended to intermolecular potentials between two molecules of any number or arrangement of atoms. On the other hand, they estimate that errors of roughly 10% in the Born–Mayer parameters may be expected from the use of the combining rules. We can see this in the comparison of the values for the lighter rare gas atoms with the values for the N_2–He, Ne, and Ar systems from the Bowers *et al.* paper.[16] We note that the Nyeland–Toennies estimates of A and b are systematically larger than the BTT values for these systems. Nevertheless, we adopt the Nyeland–Toennies Born–Mayer parameters for the N_2–Kr system.

TABLE I. Comparison of Born–Mayer parameters.

		0°		90°	
		BTT[a]	NT[b]	BTT[a]	NT[b]
N_2–He	A	455.1	639	62.84	63.1
	b	2.119	2.23	2.082	2.13
N_2–Ne	A	1450	1650	135.0	174
	b	2.175	2.23	2.080	2.15
N_2–Ar	A	1211	1870	250	354
	b	1.87	1.96	1.88	1.96
N_2–Kr	A	⋯	2890	⋯	547
	b	⋯	1.95	⋯	1.94
N_2–Xe	A	⋯	1690	⋯	399
	b	⋯	1.77	⋯	1.77

[a]Bowers, Tang, and Toennies, Ref. 16.
[b]Nyeland and Toennies, Ref. 32.

In this paper three approaches have been used to determine the dispersion contribution. The anisotropic dispersion series is given by (even order terms only for the system under study here)

$$C_{2n}(\theta)=C_{2n}^{(0)}+C_{2n}^{(2)}P_2(\cos\ \theta)+\cdots+C_{2n}^{(2n-4)}P_{2n-4}(\cos\ \theta),$$

where $C_{2n}(\theta)$ is the dispersion coefficient that corresponds to a term, in the multipole expansion of the interaction energy, of the form $-C_{2n}/R^{2n}$. The first approach (to construct the BNT8 N_2–Kr surface) uses the $C_{2n}^{(k)}$ values determined by Bowers and Tang[33] from combining rules, as was done for the N_2–He, Ne, and Ar systems. Values for the dispersion

TABLE II. Dispersion coefficients used in the N_2–Kr surfaces.[a]

	BNT8[b]	TNTA[c]	TNTB[e]	MNT[f]
$C_6^{(0)}$	100.2	100.67	97.28[d]	108.728
$C_6^{(2)}$	12.06	13.23	10.57[d]	13.015
$C_8^{(0)}$	3 037	3 224.5	3 138.8	3 156.583
$C_8^{(2)}$	2 082.8	2 055.3	2 013.8	1 809.669
$C_8^{(4)}$	−68.03	−62.50	−59.43	⋯
$C_{10}^{(0)}$	99 894	112 510	112 990	112 261.054
$C_{10}^{(2)}$	95 208.97	100 203	99 567.6	88 315.77
$C_{10}^{(4)}$	12 706.52	9 260.0	10 190	⋯
$C_{10}^{(6)}$	−710.246	−451.36	−623.65	⋯
$C_{12}^{(0)}$	3 565 755.468	⋯	⋯	5 028 409.58
$C_{12}^{(2)}$	1 151 962.128	⋯	⋯	4 022 727.664

[a]All numbers are in atomic units.
[b]From Ref. 33. The values of $C_{12}^{(0)}$ and $C_{12}^{(2)}$ for the Bowers and Tang set have been calculated using the combining rule.
[c]From Ref. 34. The TNTM surface uses the same dispersion coefficients as the TNTA with the following values for the repulsive parameters for the 0^0 orientation α=1.3687, β=0.11 845, and γ=0.006 634. These were switched back to the original Born–Mayer A and b parameters at R=4.814 65 Å.
[d]The values of $C_6^{(0)}$ and $C_6^{(2)}$ are empirical values from Meath and Kumar (Ref. 37).
[e]From Ref. 35, N_2 bond length=1.094 Å.
[f]From Ref. 39.

coefficients are given in Ref. 33 up to $C_{10}^{(6)}$. For n=6 and 8, we determined the $C_{2n}(\theta)$ from the combining rule (see for example Ref. 16),

$$C_{2n}(\theta)=\left[\frac{C_{2n-2}(\theta)}{C_{2n-4}(\theta)}\right]^3 C_{2n-6}(\theta).$$

A value of 8 for $n_{\max}$ is used in the radial dependence for the two cuts of the surface at θ=0° and θ=90°.

In the second approach (to construct the TNTA and TNTB surfaces) we use the set of Born–Mayer parameters from Nyeland and Toennies[32] and sets of *ab initio* dispersion coefficients calculated by Thakkar and co-workers at two levels of theory.[34,35] The first set of Thakkar dispersion coefficients (used to construct the TNTA surface) had been determined from dynamic polarizabilities calculated using many-body perturbation theory (MBPT) for Kr and Xe and those for N_2 by Rijks and Wormer[36] using MBPT as well. More recently, Thakkar and co-workers have reported a new set of dispersion coefficients based on the same calculations for Kr and Xe but new results for N_2 at three intramolecular distances.[35] The TNTB surface uses these new results (with N_2 at its equilibrium distance). In addition, the empirical values of $C_6^{(0)}$ and $C_6^{(2)}$ obtained from moments of the dipole oscillator strength distribution (DOSD) by Meath and Kumar[37] were used (as recommended by the authors[35]). For the TNT surfaces, the dispersion was represented by the coefficients as published, and no additional terms were calculated. A further variation using Thakkar's dispersion coefficients was considered. From the work of McCourt and coworkers on the N_2–Ar system,[4] it had been observed that the repulsive parts of the cuts of the surface at θ=0° and θ=90° should be parallel in order to better reproduce rotational relaxation cross sections. Thus, a modified surface, TNTM, has been constructed, in which the radial dependence of the repulsive wall at 90° has been shifted and added to the attractive part of the 0° cut of the TNTA surface. These points were then fit to a TT type model potential where the Born–Mayer parameter b is replaced by $\alpha R-\beta R^2-\gamma R$,[3,38]

$$V(R,\theta=0°)=A(0°)\exp[-(\alpha R-\beta R^2-\gamma R^3)]$$
$$-\sum_{n\geq 3}^{n_{\max}}\left\{1-\sum_{k=0}^{2n}\frac{[\alpha R-\beta R^2-\gamma R^3]^k}{k!}\right.$$
$$\left.\times\exp[-(\alpha R-\beta R^2-\gamma R^3)]\right\}\frac{C_{2n}(0°)}{R^{2n}}.$$

To be consistent with the number of terms included in the dispersion series, $n_{\max}$ in the damping function is restricted to a value of 5 for all three of the TNT surfaces.

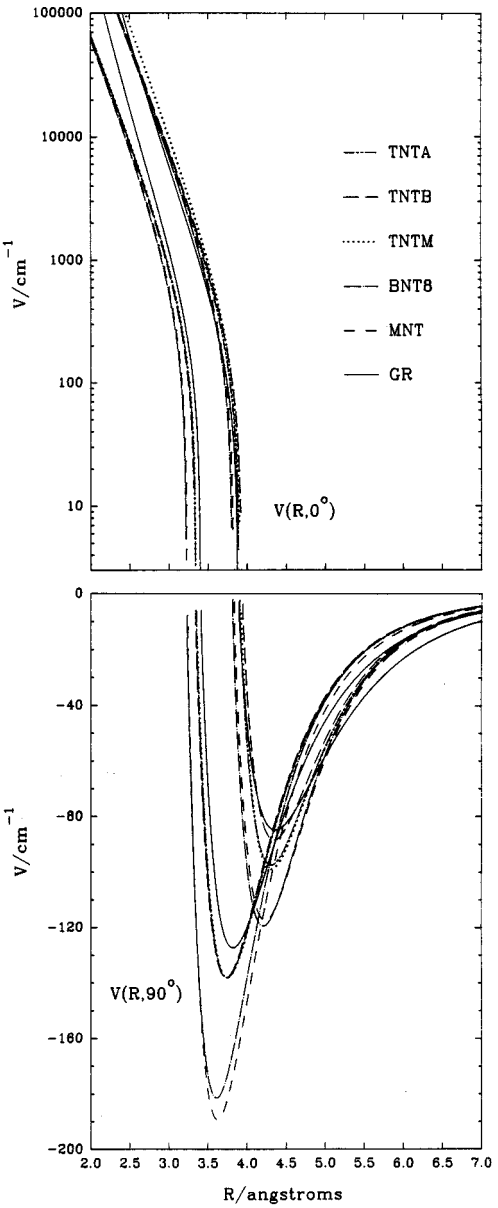

FIG. 1. Parallel (θ=0°) and perpendicular (θ=90°) cuts of the N_2–Kr potential energy surfaces, (a) the repulsive walls and (b) the attractive bowls.

TABLE III. Characteristics of the N_2–Kr surfaces.[a]

	GR	TNTA	TNTB	TNTM	BNT8	MNT
$\epsilon(90°)$	127.44	138.18	138.13	138.18	181.48	189.31
$R_m(90°)$	3.82	3.74	3.73	3.74	3.61	3.62
$\sigma(90°)$	3.40	3.34	3.33	3.34	3.22	3.23
$\epsilon(0°)$	84.96	97.49	88.54	99.04	119.54	117.52
$R_m(0°)$	4.36	4.31	4.34	4.30	4.21	4.23
$\sigma(0°)$	3.88	3.90	3.93	3.91	3.81	3.83
$\Delta\epsilon$	42.48	40.69	49.59	39.14	61.94	71.79
ΔR_m	0.54	0.57	0.61	0.56	0.60	0.61
$\Delta\sigma$	0.48	0.56	0.60	0.57	0.59	0.60
ΔR_{1000}	0.35	0.49	0.51	0.52	0.50	0.51
ΔR_{5000}	0.30	0.46	0.48	0.52	0.48	0.48
$V_0(R)$ parameters						
ϵ	106.70	101.01	95.00	101.03	125.09	128.28
R_m	4.04	4.08	4.10	4.09	3.98	3.99
σ_0	3.60	3.67	3.70	3.70	3.58	3.59

[a]Energies are in cm^{-1} and distance are in Å.

The third approach (used to construct the MNT surface) uses estimates of the dispersion coefficients from McCourt.[39] These were determined by extrapolating plots of C_6 and C_8 vs the polarizability of the noble gas atom to the polarizability of Kr. The $C_6^{(2)}$ and $C_8^{(2)}$ coefficients were obtained from plots of $C_{2n}^{(0)}/C_{2n}^{(2)}$, and for C_{10} and C_{12} the combining rules were used. The MNT surface contains only P_0 and P_2 terms, and thus the $C_{2n}(\theta)$ series is truncated at the $C_{2n}^{(2)}P_2(\cos\theta)$ term and $n_{\max}$ in the damping function is restricted to a value of 6.

Table II lists the various sets of dispersion coefficients used in these four new anisotropic N_2–Kr potential energy surfaces. Cuts of the potential energy surfaces are shown in Fig. 1. The points of interest on each of the surfaces are the energy minima at the perpendicular ($\theta=90°$) and parallel ($\theta=0°$) configurations of the N_2–Kr dimer and the values of σ, (where $R=\sigma$ corresponds to $V=0$) for these configurations. The anisotropies are expressed as the difference between a characteristic of the $\theta=0°$ and $\theta=90°$ cuts,

$$\Delta\sigma=\sigma(\theta=0°)-\sigma(\theta=90°),$$

$$\Delta R_m=R_m(\theta=0°)-R_m(\theta=90°),$$

$$\Delta\epsilon=\epsilon(\theta=0°)-\epsilon(\theta=90°),$$

and

$$\Delta R_V=R_V(\theta=0°)-R_V(\theta=90°),$$

where $\Delta R_V(\theta)$ is the radial distance corresponding to a potential energy of V at a particular angle θ. A summary of the potential characteristics for these N_2–Kr potentials is listed in Table III. Following Ref. 4, we characterize the anisotropy of the PES not only with the values of R_m, ϵ, and crossing point σ at the two extremes ($\theta=0°$ and $\theta=90°$), but also include the values of the differences in position of the repulsive wall of the PES at the two extreme geometries for two energies $V=1000$ and 5000 cm^{-1} to provide an indication of the anisotropy for $R<\sigma$.

The BNT8 and MNT potentials have an isotropic component that is deeper and located further inward relative to the isotropic component of the other potentials. The model potentials of the TT type that we constructed all have a larger anisotropy in the location of the potential minimum than the Rotzoll (GR) potential. They are more anisotropic in the region where the potential vanishes, as well as high up in the repulsive wall, compared to the Rotzoll potential. The anisotropy in the well depth is least for TNTM and largest for BNT8 and MNT. The Rotzoll well depth anisotropy is comparable to that of TNTA and TNTM.

III. CALCULATIONS OF THE COLLISION CROSS SECTIONS

McCourt and co-workers provide a detailed derivation of the collision cross sections related to the transport and relaxation properties which are used in testing nonreactive potential surfaces.[40,41] From the Boltzman equation, the Chapman–Enskog procedure[42] can be used to obtain classical definitions of the kinetic theory cross sections (see also Refs. 43 and 44). The nomenclature used to label the collision cross sections specifies the nature of the collisional process which contributes to the phenomenon. In general, a collision or effective cross section is given by

$$\mathfrak{S}\begin{pmatrix} p & q & s & t & | & k \\ p' & q' & s' & t' & | & k' \end{pmatrix}_{kk''}.$$

The indices p, q, s, t represent the precollisional (primed) and postcollisional (unprimed) tensorial ranks or powers of the microscopic polarizations which are coupled. p denotes the p-fold tensor product of the reduced peculiar velocity $\mathbf{W}=(m/2kT)^{1/2}\mathbf{v}$, q denotes the tensorial rank in the molecular angular momentum $\mathbf{j}$. The s and t indices denote the scalar dependencies of the cross section on the translational and reduced rotational energy. The various k's label which collision partner the polarizations belong to; k, k', $k''=A$ or B. When the pre- and postcollisional values are identical and changes in only one partner are relevant, the cross section can be abbreviated, $\mathfrak{S}(pqst|k)_{kk''}$. For the unlike interactions of N_2 and Kr, $A=N_2$ and $B=$Kr.

The temperature-dependent cross sections were calculated for each PES from fully classical trajectories using the

code developed by Dickinson and Lee[45] without any modifications. In a study of the N_2–He system,[13] the same code gave results similar to those of the close-coupling method. The agreement increases with temperature, as more rotational states of N_2 are occupied. The classical approach and the Dickinson–Lee code are expected to provide accurate results for the N_2–Kr and N_2–Xe systems. Wong has described this code in detail,[12] and the following is a brief summary of the method. Where mentioned, energy ranges, number of quadrature points, etc. apply to the N_2–Kr case.

The set of variables used as initial conditions are dictated by the coordinates used to write Hamilton's equations of motion and the fewer the equations of motion, the more economical it is to run the code. In Cartesian coordinates, twelve variables are needed to uniquely describe a diatom–atom system. The rigid rotor approximation and action angle coordinates can be used to reduce this set. Miller defines the action angle coordinates in terms of Cartesian coordinates and writes the classical Hamiltonian in the center-of-mass frame as[46]

$$H(P,l,j;R,q_l,q_j)=(P^2+l^2/R^2)/2\mu+Bj^2+V(R,\cos\,\theta),$$

where P is the center-of-mass momentum, R is the separation of centers of mass of the colliding species, and μ is the reduced mass. The orbital angular momentum **l** is defined as the angular momentum of the atom about the center of mass of the rotor. The rotational energy of the rotor is given by the rotational constant B and angular momentum **j**. The potential energy function $V(R,\cos\theta)$ is written in terms of R and the cosine of the angle θ between the rotor axis and the line of centers. The angular dependence of the PES can be written in terms of the action angle coordinates as follows:

$$\cos\,\theta=-\cos\,q_l\,\cos\,q_j+[(l^2+j^2-J^2)/2lj]\sin\,q_l\,\sin\,q_j,$$

where the total angular momentum is **J**. The coordinates q_l and q_j are the angles conjugate to **l** and **j**, respectively.

The total energy is selected first from a set of values determined from a Clenshaw–Curtis quadrature in three ranges as described by Dickinson and Lee[47] (see also Ref. 48). In general, the middle range covers energies of about one to ten times the well depth of the PES.[49] The lower and higher ranges are extended far enough to incorporate the proper Boltzmann distributions for the temperatures desired. For the systems studied, the energy mesh used follows the extensive work of Wong and McCourt (see for example Ref. 12). The high energy range is composed of five energies from 30 000 to 2 500 cm^{-1}, nine points are used between 2500 and 150 cm^{-1} and three points cover the low energy range down to 40 cm^{-1}.

The initial rotational energy E_r and the initial translational (kinetic) energy E_k are partitioned from the total energy E_{tot} using

$$\omega=(E_r-E_k)/E_{tot}.$$

A 12-point Gaussian quadrature is used for ω with the most positive value neglected, since the extremely low kinetic energy would make for an expensive trajectory to calculate. Wong found these eleven points to adequately describe the rotational states of N_2 and CO_2 in his work on the N_2–light noble gas atom[12,50] and CO_2–He (Ref. 51) systems [and also for O_2 in He and Ne (Ref. 52)].

At each E_{tot} and ω, the initial relative orientation of the rotor and atom is described by the values of q_l, q_j and the angle λ between **j** and **l**. The conjugate angles q_l and q_j are selected from an 8 to 12 point trapezoidal rule and an 8 to 12 point quadrature is used for λ. The impact parameter b can be defined as the distance of closest approach if there were no intermolecular forces and is specified in quadratures over two ranges. These ranges are divided by the rainbow value of the impact parameter b_r where a maximum is observed in the scattering angle as a function of b. For $b_{in}<b_r$, an 8 to 12 point quadrature is used. For $b_{out}>b_r$, an 8 to 12 point quadrature is also used but the points are selected so that the maximum impact parameter b_{max} corresponds to a scattering angle of roughly one degree. Initial runs over a range of b were made with two points in each of the orientation variables to find b_r at each set of E_{tot} and ω.

Once a proper value for b_r is chosen and the range of b_{out} selected, the optimum number of values in the orientation variable set is picked. Initially, a control set of trajectories at a high E_{tot} and low ω (high translation energy) was run with a reliable set of impact parameters and 12 points in each of the orientation angles. Then the number of points is reduced until a minimum set of q_l, q_j, and λ are found which best reproduces the set of partially averaged cross sections from the control. This minimum set was then used for all b, ω, and E_{tot}.

This method for testing for convergence was accompanied by comparing energy dependent cross sections which are related by time reversal symmetry (TRS). TRS cross sections are related by their similar dependence on the initial and final velocities and angular momenta. For example, the following energy-dependent production cross sections are related by whether the dependence is on the initial velocity $\mathbf{v}'$ and final angular momentum **j** or on **v** and $\mathbf{j}'$,

$$\mathfrak{S}\begin{pmatrix}0&2&0&0\\2&0&0&0\end{pmatrix}_E=\int\langle P_2(\mathbf{v}'\cdot\mathbf{j})\rangle_E d\tau$$

and

$$\mathfrak{S}\begin{pmatrix}2&0&0&0\\0&2&0&0\end{pmatrix}_E=\int\langle P_2(\mathbf{v}\cdot\mathbf{j}')\rangle_E d\tau,$$

where $d\tau$ is the integration element for the averages over ω and b. The integrand represents the functional description of the collision process averaged over q_l, q_j, and λ and can be referred to as an opacity function. Although these are energy-dependent functions, a similar nomenclature to that for temperature dependent cross sections is used to illustrate the pertinent polarizations. The inverted order of the indices identifies TRS cross sections. Additional comparisons can be made between two cross sections that depend on the same collisional process but involve different functional forms. These cross sections differ in the explicit form of the opacities used. The viscosity cross section $\mathfrak{S}_\eta$ is calculated with two functionally different opacity functions and are also used to test for convergence.

All surfaces were used for trajectory calculations (no surface was reported by Kistemaker and de Vries for the N_2–Kr system) even though only the TNTA surface is in excellent agreement with the B_{12} data. This will permit a further comparison of the various methods used to create the full surfaces. For example, the effects of different attractive contributions to the various TT surfaces can be examined.

We considered carefully the selection of an optimum set of q_l, q_j, and λ and found that 8 points in each of q_l, q_j, and λ were sufficient. This is in contrast to our study of CO_2–Ar surfaces,[53] in which we had to increase the number of points used in each of the orientation angles to 12 points in order to reduce the error in the TRS and opacity-related cross sections. On the order of 2 million trajectories were used for each of the N_2–Kr surfaces. All calculations were done on IBM RISC/6000 model 560 and model 365 workstations.

IV. RESULTS

Usually, a proposed surface must first predict experimental interaction second virial coefficient data before consideration in a trajectory study since virial coefficient calculations are inexpensive. Our interests are in finding a reliable N_2–Kr surface and understanding the relation between the PES and the gas phase NMR relaxation experiments conducted in our laboratory. Thus, we report the results of all six surfaces regardless of their abilities in predicting virial coefficients. In particular, calculated values for interaction second virial coefficients, diffusion coefficients, mixture viscosity, thermal conductivity, and two NMR cross sections are presented for each surface. In addition to the quantities described below, 45 different cross sections were calculated at 100–800 K, including production cross sections for each of the six N_2–Kr surfaces. Values for the cross sections not mentioned here can be obtained from the authors and Ref. 54.

A. Interaction second virial coefficient, B_{12}

From the virial expansion (in inverse powers of the molar volume) of the equation of state,

$$\frac{P\bar{V}}{RT}=1+\frac{B(T)}{\bar{V}}+\frac{C(T)}{\bar{V}^2}+\cdots$$

the temperature-dependent functions $B(T)$, $C(T)$,... are referred to as the second, third,... virial coefficients. For a binary mixture, the experimental second virial coefficient B_{mix} is given by

$$B_{\mathrm{mix}}=x_1B_{11}+2x_1x_2B_{12}+x_{22}B_{22},$$

where the quantities with subscripts 11 and 22 are the second virial coefficients for the pure gases and B_{12} is the interaction second virial coefficient for the unlike interaction. In general, the interaction second virial coefficient can be calculated by integrating the PES over relative orientations, and for a linear molecule atom system, the following is used (see for example, Ref. 55),

$$B_{12}(T)=B_{12}^{\mathrm{class}}(T)=N_0\pi\int_0^\infty dR\ R^2\int_{-1}^{1}d\ \cos\ \theta \times\left\{1-\exp\left[\frac{-V(R,\cos\ \theta)}{kT}\right]\right\},$$

where R is the center of mass separation, θ is the angle between the rotor molecular axis and the line of centers, and $V(R,\cos\theta)$ is the interaction potential energy surface. The first translational and rotational quantum corrections can also be included. These add integrals over the PES to the classical B_{12} values so that

$$B_{12}(T)=B_{12}^{\mathrm{class}}(T)+B_{12}^{\mathrm{trans}}(T)+B_{12}^{\mathrm{rot}}(T)$$

and have been used for calculations of B_{12}. These corrections are given by[55,56]

$$B_{12}^{\mathrm{trans}}=\frac{N_0\pi\hbar^2}{24\mu(kT)^3}\int_0^\infty dR\ R^2\int_{-1}^{1}d\ \cos\ \theta \times\left\{\exp\left[\frac{-V(R,\cos\ \theta)}{kT}\right]\right\}\left[\frac{\partial V(R,\cos\ \theta)}{\partial R}\right]^2$$

and

$$B_{12}^{\mathrm{rot}}=\frac{N_0\pi}{24(kT)^3}\int_0^\infty dR\ R^2\int_{-1}^{1}d\ \cos\ \theta \times\left\{\exp\left[\frac{-V(R,\cos\ \theta)}{kT}\right]\right\}\left(\frac{\hbar^2}{\mu R^2}+\frac{\hbar^2}{l_I}\right) \times\left[\sum_{L=0}^{\infty}L(L+1)V_L(R)P_L(\cos\ \theta)\right],$$

where $V_L(R)$ are the radial coefficients of the Legendre expansion of $V(R,\cos\theta)$ in terms of $\cos\theta$,

$$V(R,\cos\ \theta)=\sum_L V_L(R)P_L(\cos\ \theta)$$

and l_I is the rotor's rotational moment of inertia. Due to the angle-averaged nature of the virial coefficient and its independence of **j**, it is primarily sensitive to the isotropic part of the PES.

Figure 2 and Table IV show the results of the calculation of B_{12} including the rotational and translational quantum corrections, as a function of temperature for each of the N_2–Kr surfaces. The TNTA surface provides the best agreement with Brewer's experiments.[21] The various TNT surfaces produce B_{12} values which slightly overestimate the experimental values. The other surfaces underestimate the experiment and fall outside of the error bars of the experiment (±1 $\mathrm{cm}^3/\mathrm{mol}$).[21] These values of B_{12} reflect the deeper wells of the MNT and BNT8 surfaces. The poor results from the GR surface may be due to its LJ(12,6) form. One could adjust the angle-averaged parameters, $\bar{\epsilon}$ and R_m, so that agreement is obtained. However, since the anisotropy had been adjusted to reproduce the molecular beam experiments, attempts at adjusting a and b have to be done in such a way as to retain the good agreement with the scattering experiments.

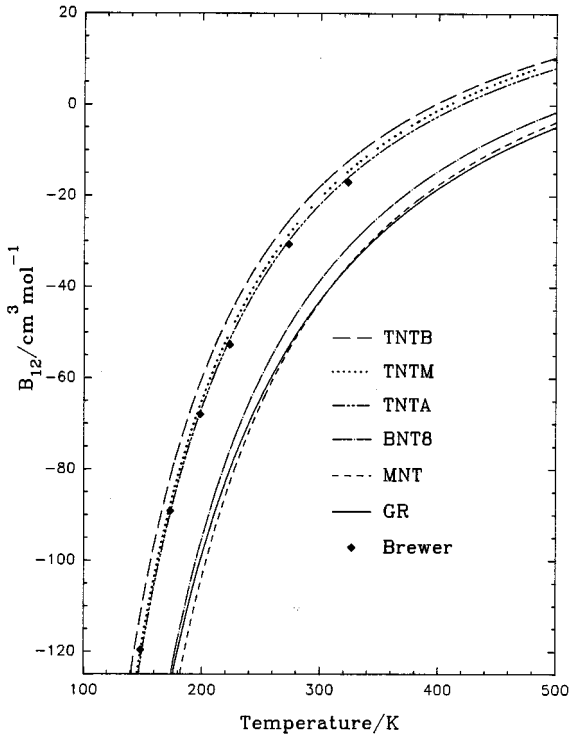

FIG. 2. Temperature dependence of the interaction second virial coefficient in N_2–Kr. The experimental error is ± 0.1 cm^3 mol^{-1} as reported by Brewer (Ref. 21).

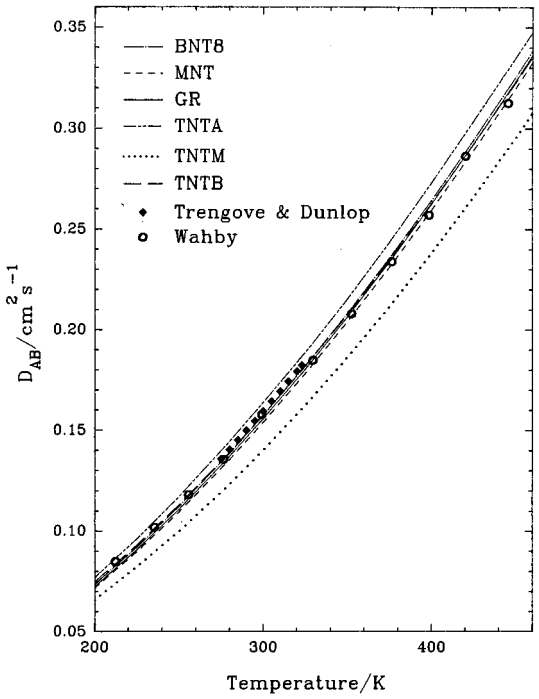

FIG. 3. Comparison of calculated and experimental diffusion coefficients for N_2–Kr. The data from Trengove and Dunlop have been calculated from the reported quadratic temperature dependence in increments of 5 K and have an uncertainty of less than 0.1% (Ref. 23). Wahby reports an uncertainty of about $\pm 1.5\%$ (Ref. 24).

B. Diffusion coefficients

Within the first order Chapman–Cowling approximation[42] of a binary mixture, the binary diffusion coefficient is given by[40]

$$D_{AB}=kT/[m_A\rho_A L_0 \bar{v}\mathfrak{S}(1000|A)_{AB}],$$

where Boltzmann's constant is given by k, $\bar{v}$ is the mean relative speed, $(8kT/\pi\mu)^{1/2}$, where μ is the reduced mass of the pair, L_0 is Loschmidt's number ($2.686\,763\times10^{25}$ molecules m^{-3}) and ρ_A is the density of species A in amagat. The notation used in the diffusion cross section, $\mathfrak{S}(1000|A)_{AB}$ is an extension of the notation described above where now $A=N_2$ and $B=$Kr. This cross section is not very sensitive to the anisotropic part of the PES, since it has only a small contribution from inelastic collisions. Using the classical trajectory results for the diffusion cross sections, the diffusion coefficient has been calculated for each of the surfaces.

There are two sets of experimental diffusion data in the literature. The experimental values for the diffusion coefficient of Trengove and Dunlop[23] were obtained as a function of temperature and mole fraction of Kr, x_{Kr}, and the values of D_{AB} were obtained from extrapolation to $x_{Kr}=0$. These values were then fit to a second order polynomial in temperature[23] and the values calculated from the fit are shown in Fig. 3. The values reported by Wahby[24] were not extrapolated to $x_{Kr}=0$ and thus contain a small contribution from a finite value of x_{Kr} (the ''almost Lorentzian'' results). They were also fit to a polynomial in temperature, however, we used the actual values reported in the original paper.[24] The small differences between the two experimental data sets are not significant since the various surfaces predict similar values of D_{AB}. The calculated values are compared with experimental results in Fig. 3. The predictions from the TNTA surface agree best with the data of Trengove and Dunlop, while the MNT, GR, BNT8, and TNTB surfaces repro-

TABLE IV. Comparison of calculated and experimental values for the interaction second virial coefficient.

T/K	GR	TNTA	TNTB	TNTM	MNT	BNT8	Experiment[a]
148.15	−168.17	−122.06	−112.12	−119.89	−183.74	−169.58	−119.58
173.15	−128.04	−89.804	−81.910	−87.882	−136.72	−126.00	−89.14
198.15	−100.44	−67.681	−61.126	−65.918	−105.45	−96.897	−67.92
223.15	−80.339	−51.607	−45.994	−49.953	−83.223	−76.144	−52.68
273.15	−53.099	−29.898	−25.516	−28.382	−53.829	−48.618	−30.71
323.15	−35.570	−15.992	−12.380	−14.559	−35.353	−31.272	−17.08

[a]Reference 21.

duce this data and those of Wahby. The TNTM results are too low. We note that the diffusion coefficient alone is not a sufficient test of an anisotropic PES.

C. Mixture viscosity

The first order Chapman–Cowling approximation expresses the mixture viscosity, $\eta_{\rm mix}$, as[40,57(a)]

$$\eta_{\rm mix}=\frac{kT}{v\Delta_{AB}}\left\{x_A^2\mathfrak{S}(2000|B)_{AB}+x_Ax_B\left[\sqrt{2}y_A\mathfrak{S}(2000|B)_{BB}-2\mathfrak{S}\begin{pmatrix}2000|A\\2000|B\end{pmatrix}_{AB}+\sqrt{2}y_B\mathfrak{S}(2000|A)_{AA}\right]+x_B^2\mathfrak{S}(2000|A)_{AB}\right\}$$

where

$$\Delta_{AB}=[\sqrt{2}y_Bx_A\mathfrak{S}(2000|A)_{AA}+x_B\mathfrak{S}(2000|A)_{AB}]\times[x_A\mathfrak{S}(2000|B)_{AB}+\sqrt{2}x_Bv_A\mathfrak{S}(2000|B)_{BB}]-x_Ax_B\left\{\mathfrak{S}\begin{pmatrix}2000|A\\2000|B\end{pmatrix}_{AB}\right\}^2$$

and x_A and x_B are the mole fractions for species A and B. These cross sections, given in the standard notation, clearly do not involve angular momentum changes and are not expected to be noticeably sensitive to the anisotropy of the potential surface. The y_α factors are functions of the masses, $y_\alpha=(m_\alpha/M_{\rm tot})^{1/2}$.

Experimental values of η for pure Kr and N_2 have been used. This forces agreement between theory and experiment for $x_{N_2}=0$ and 1. Thus it is only the values of $\eta_{\rm mix}$ as a function of x_{N_2} that are important in the comparison. Figure 4 shows the results at three temperatures. Experimentally, the $\eta_{\rm mix}$ values deviate from a linear dependence on x_{N_2}, with larger values (than a linear dependence) for x_{N_2} in the midrange. All but one of the surfaces reproduce the general dependence on the N_2 mole fraction at all five temperatures. The TNTM surface fails to produce values within the experimental error.

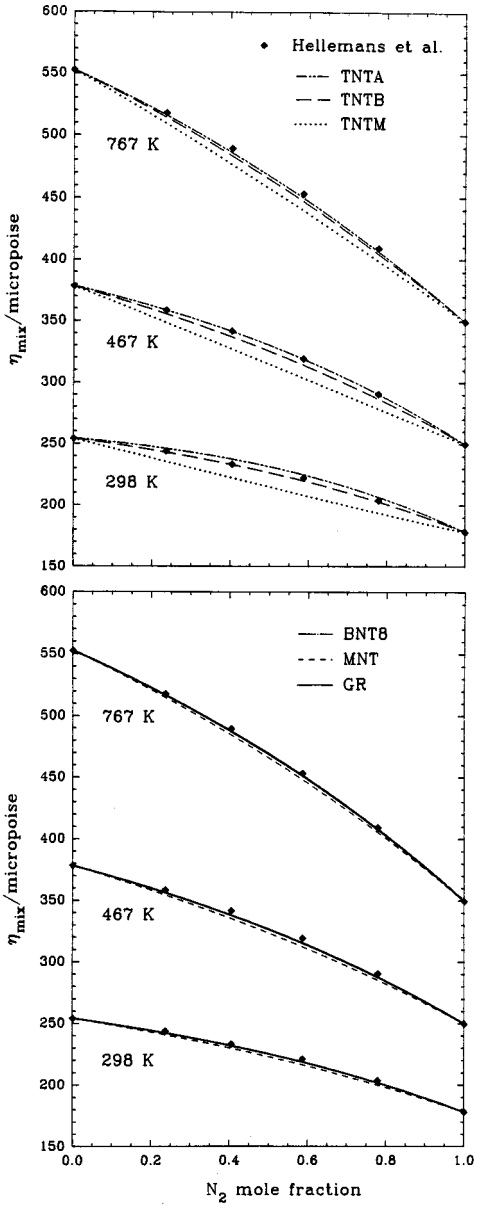

FIG. 4. Temperature and mole fraction dependence of the mixture viscosity in N_2–Kr. Predictions from the (a) TNTA, TNTB, TNTM and (b) BNT8, MNT, GR surfaces are compared with the experimental data of Hellemans *et al.* (standard deviation of 0.33%) (Ref. 25).

D. Thermal conductivity

In contrast to diffusion and viscosity, the thermal conductivity has a contribution from the molecular angular momentum of the rotor. McCourt and Liu have discussed the first order Chapman–Cowling expression for the thermal conductivity coefficient, $\lambda_{\rm iso}$.[57(b)] Within this approximation, the thermal conductivity coefficient depends on the following cross sections:

$$\mathfrak{S}(1001|A)_{AB}\quad\mathfrak{S}(1010|A)_{AB}$$

$$\mathfrak{S}\begin{pmatrix}1\,0\,0\,1\,|A\\1\,0\,1\,0\,|A\end{pmatrix}_{AB}\quad\mathfrak{S}\begin{pmatrix}1\,0\,1\,0\,|A\\1\,0\,1\,0\,|B\end{pmatrix}_{AB}$$

$$\mathfrak{S}\begin{pmatrix}1\,0\,0\,1\,|A\\1\,0\,1\,0\,|B\end{pmatrix}_{AB}\quad\mathfrak{S}(1010|B)_{AB}.$$

The cross sections in the first column depend on the rotational state of N_2 in N_2–Kr mixtures, for example. The pure noble gas cross section $\mathfrak{S}(1000|B)_{BB}$ and the pure gas cross sections for the linear rotor $\mathfrak{S}(1000|A)_{AA}$,

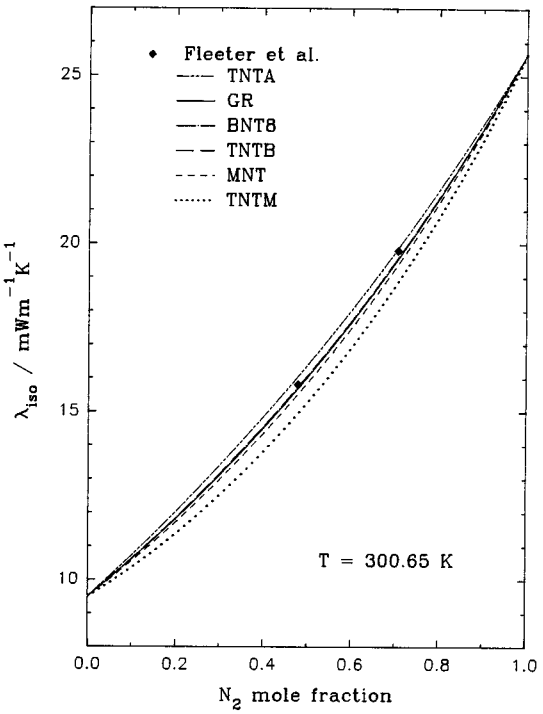

FIG. 5. Mole fraction dependence of the thermal conductivity coefficient from the N_2–Kr potentials and the experimental data of Fleeter *et al.* (±0.3% accuracy) (Ref. 26) at 300.65 K.

$\mathfrak{S}(0001|A)_{AA}$, and $\mathfrak{S}(^{0001|A}_{0010|A})_{AA}$ are also needed. Like the mixture viscosity, the calculation of the mole fraction dependence for λ_{iso} is fixed by the pure gas cross sections in the limit of the pure gases.

Calculated values of λ_{iso} as a function of the N_2 mole fraction are compared with the experimental data of Fleeter *et al.*[26] in Fig. 5. All but the MNT and TNTM surfaces predict the experimental points, with the GR, BNT8, and TNTB surfaces giving nearly identical values.

E. NMR cross sections

Measurements of the spin-lattice relaxation time, T_1, from nuclear magnetic resonance (NMR) experiments provide two independent cross sections which are associated with the collisional effects on the molecular rotational angular momentum, **j**. When the relaxation of a quadrupolar nucleus is dominated by the coupling between the nuclear electric quadrupole moment and the molecular electric field gradient at the nucleus, the observed T_1 is related to the effective cross section $\mathfrak{S}'(0\hat{2}00|\mathrm{A})_{\mathrm{AB}}$ by[58]

$$T_1=\frac{160I^2(2I-1)}{3(2I+3)}\left(\frac{\hbar}{eqQ}\right)^2\rho\bar{v}\mathfrak{S}'(0\hat{2}00|A)_{AB},$$

where I is the nuclear spin quantum number, $eqQ/\hbar$ is the nuclear quadrupole coupling constant, ρ is the number density of the collision partner, and $\bar{v}$ is the mean relative speed. The electronic coupling affects the populations of the nuclear magnetic spin states since the magnetic moment is directed along the axis of the nuclear electric charge distribution. Using a classical treatment, Gordon has shown this cross section to depend only on the reorientation of the molecular angular momentum[58]

$$\mathfrak{S}'(0\hat{2}00|A)_{AB}=(3/2)\int\langle\sin^2\theta_j\rangle_i 2\pi b\,db,$$

where θ_j is the angle between the angular momentum before and after a collision. The brackets imply an average over the internal states of the molecules. The capped integer in the symbol for the cross section denotes the use of normalized angular momentum. That is, the cross section can be written as

$$\mathfrak{S}'(0\hat{2}00|A)_{AB}=(3/2)\int\langle 1-[\mathbf{J}'\cdot\mathbf{J}/(J'J)]^2\rangle_i 2\pi b\,db.$$

This relation was arrived at from a classical treatment of an autocorrelation function of a unit vector **u** fixed to the rotating molecule which gave the following equality:[58]

$$\int_0^\infty\langle P_2[\mathbf{u}(0)\cdot\mathbf{u}(t)]\rangle dt=(1/4)[\rho\bar{v}\mathfrak{S}'(0\hat{2}00|A)_{AB}]^{-1}.$$

The same cross section can be obtained from dipole–dipole dominated relaxation or when the relaxation is dominated by chemical shift anisotropy.

In depolarized Rayleigh light scattering, the scattered light is coupled to the rotation of the molecule by the polarizability tensor and collisional changes in the angular momentum affect the resultant spectrum. The Fourier transform of the autocorrelation function, $C(t)$, for the traceless part of the transition polarizability tensor is directly related to the normalized band shape[59]

$$I(\omega)=(1/2\pi)\int C(t)\exp(-i\omega t)dt,$$

where[59]

$$C(t)=\frac{\langle\mathrm{Tr}\ \beta(0)\cdot\beta(t)\rangle}{\langle\mathrm{Tr}\ \beta(0)\cdot\beta(0)\rangle},$$

where β is the traceless part of the transition polarizability matrix. In general, the cross section derived from the collisional line broadening of the depolarized Rayleigh line is

$$\mathfrak{S}(0\hat{2}00|A)_{AB}=4I(0)/\rho\bar{v}c\int_{\mathrm{band}}I(\omega)d\omega,$$

where $I(0)$ corresponds to the $\Delta j=0$ part of the spectrum. When the probe molecule is linear, the correlation function can be related to a vector **u** rigidly attached to the molecule,[59]

$$C(t)=\frac{\langle\mathrm{Tr}\ \beta(0)\cdot\beta(t)\rangle}{\langle\mathrm{Tr}\ \beta(0)\cdot\beta(0)\rangle}=\langle P_2[\mathbf{u}(0)\cdot\mathbf{u}(t)]\rangle.$$

When the collision partner is a molecule, its own angular momentum contributes to the correlation function and the relevant cross section $\mathfrak{S}(0\hat{2}00|\mathrm{A})_{\mathrm{AB}}$ is defined as

$$\mathfrak{S}(0\hat{2}00|A)_{AB}=\mathfrak{S}'(0\hat{2}00|A)_{AB}+\mathfrak{S}''(0\hat{2}00|A)_{AB}$$

and

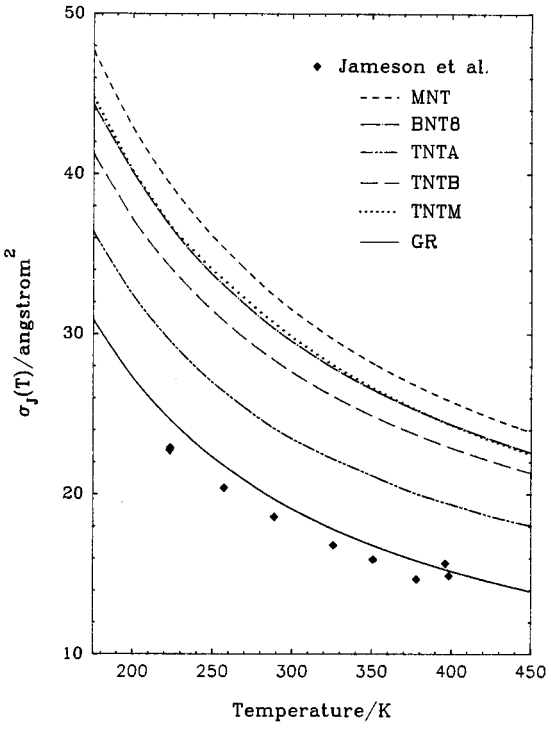

FIG. 6. Comparison of calculated and experimental values of σ_J [$\mathfrak{S}(0100|A)_{AB}$] in N_2–Kr. The experimental data was obtained in our laboratory (Ref. 27) and has an uncertainty of 1 Å^2.

$$\mathfrak{S}''(0\hat{2}00|A)_{AB}=(3/2)\int\left\langle\frac{(\mathbf{J}\cdot\mathbf{J_p})^2}{(JJ_p)^2}-\frac{(\mathbf{J}\cdot\mathbf{J}'_\mathbf{p})^2}{(JJ'_p)^2}\right\rangle_i 2\pi b\ db,$$

where $\langle\ \rangle_i$ stands for an average over the internal states of the molecule. In a linear molecule–atom system the spherical collision partner does not directly contribute so that

$$\mathfrak{S}(0\hat{2}00|A)_{AB}=\mathfrak{S}'(0\hat{2}00|A)_{AB}.$$

Therefore, in this case,

$$\mathfrak{S}'(0\hat{2}00|A)_{AB}\equiv\mathfrak{S}(0\hat{2})\equiv\sigma_{\theta,2}\equiv\mathfrak{S}_{\mathrm{DPR}}.$$

That is, the same cross section that describes the collisional contribution to the quadrupolar, dipole–dipole and chemical shift anisotropy mechanisms in NMR spin relaxation can also be obtained from depolarized Rayleigh experiments.

Note that when the cross section is determined from DPR experiments, the results depend on a normalization factor (the total area of the band). Since in NMR, the cross section is related to the observable (T_1) by known constants and variables, spin relaxation experiments are expected to yield values for $\mathfrak{S}'(0\hat{2}00|\mathrm{A})_{\mathrm{AB}}$ with a smaller uncertainty than DPR experiments. Furthermore, DPR scattering can have contributions from long-lived dimers which could be substantial at the lower temperatures, making direct comparisons with CT results difficult, as has been suggested earlier[60] and suspected to be important in the N_2–Ar case.[4] For the $^{14}N_2$ molecule the relaxation of the ^{14}N nucleus in the gas phase is completely dominated by the quadrupolar mechanism and the quadrupole coupling constant is well known. Thus, it is possible to obtain $\mathfrak{S}'(0\hat{2}00|\mathrm{A})_{\mathrm{AB}}$ directly from spin relaxation experiments.

Nuclear spin relaxation can also be affected by the molecular rotation when a magnetic coupling exists between the nuclear magnetic moment and the magnetic moment associated with the molecular rotation. The spin–rotation mechanism is important for nuclei with a spherical charge distribution (spin 1/2). The cross section related to this mechanism, $\mathfrak{S}(0100|A)_{AB}$, can be related to the relaxation time through the spin–rotation coupling constant, C_{eff}. This constant is related to the components of the spin–rotation coupling tensor, which is a 2nd rank property. For a linear molecule C_{eff} is the perpendicular component of the spin–rotation tensor and the relation between the relaxation time and the cross section is

$$T_1=\frac{3\hbar^2}{2C_{\mathrm{eff}}^2IkT}\,\rho\bar{v}\mathfrak{S}(0100|A)_{AB}.$$

Using an approach similar to that used for the quadrupolar mechanism, Gordon[58] has shown

$$\mathfrak{S}(0100|A)_{AB}=(1/2\langle J^2\rangle)\int\langle(\mathbf{J}'-\mathbf{J})^2\rangle_i 2\pi b\ db.$$

The cross section $\mathfrak{S}(0100|A)_{AB}$ is also known as σ_J. The ^{15}N spin in the $^{15}N_2$ molecule in the gas phase is completely dominated by the spin rotation mechanism. The spin rotation constant for the $^{15}N_2$ molecule can be derived from the absolute ^{15}N shielding scale which relates the shielding in the N_2 molecule to the known absolute shielding in the primary reference molecule, NH_3. The absolute shielding provides the perpendicular component of the spin rotation tensor which is the only nonvanishing component in the case of the linear molecule. Thus, it is possible to determine

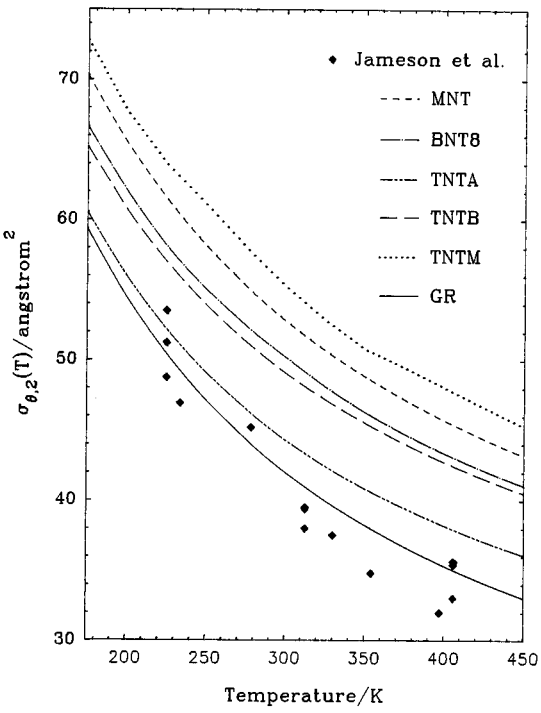

FIG. 7. Comparison of calculated and experimental values of $\sigma_{\theta,2}$ [$\mathfrak{S}(0\hat{2}00|A)_{AB}$] in N_2–Kr. The experimental data was obtained in our laboratory (Ref. 28) and has an uncertainty of 1 Å^2.

TABLE V. Comparison of calculated and experimental values for the NMR cross sections.[a]

T/K	GR	TNTA	TNTB	TNTM	MNT	BNT8	Experiment[b]
σ_J							
223.1	24.651	29.558	34.162	36.733	39.325	39.310	22.7
223.3	24.631	29.536	34.140	36.707	39.298	39.283	22.9
257.0	21.735	26.333	30.776	33.304	35.292	35.300	20.3
288.5	19.682	24.088	28.341	30.643	32.364	32.393	18.6
325.7	17.807	22.172	26.088	28.038	29.642	29.677	16.8
350.6	16.790	21.127	24.854	26.600	28.150	28.181	15.9
377.8	15.842	20.017	23.697	25.256	26.749	26.775	14.7
396.0	15.285	19.453	23.014	24.465	25.921	25.943	15.7
398.2	15.222	19.391	22.935	24.375	25.826	25.848	14.9
$\sigma_{\theta,2}$							
225.0	50.441	52.180	56.989	63.932	61.486	60.784	48.8,53.5,51.2
233.5	49.233	51.044	55.872	63.023	60.270	59.606	46.9
278.1	44.010	46.173	50.991	57.648	54.901	54.390	45.2
312.3	40.953	43.316	48.094	54.025	51.695	51.243	38.0,39.4,39.5
329.7	39.628	42.087	46.829	52.435	50.291	49.847	37.5
353.8	37.991	40.591	45.261	50.590	48.550	48.106	34.8
397.0	35.480	38.338	42.858	48.220	45.860	45.440	32.0
405.7	35.035	37.925	42.429	47.719	45.378	44.962	33.0,35.4,35.6

[a]Cross sections are in Å^2.
[b]Experimental values obtained in our laboratory.

$\mathfrak{S}(0100|A)_{AB}$ for the N_2–Kr system directly from spin relaxation experiments in the mixture. Both the $^{15}N_2$ and $^{14}N_2$ relaxation measurements in the gas phase have been done in our laboratory and reported earlier.[27,28]

Examination of Figs. 6 and 7 shows that similar trends are observed in the calculated σ_J and $\sigma_{\theta,2}$ based on the N_2–Kr surfaces studied: in all cases, the relative ordering of cross section magnitudes decreases from MNT, BNT8, TNTA to GR. The ordering of the various versions of the TNT surface has the TNTA as the lowest, followed by the TNTB and the TNTM giving the cross sections greatest in magnitude.

The best agreement for the spin–rotation cross section σ_J is provided by the GR surface which only very slightly overestimates the experimental values at the lower temperatures. Aside from the GR surface, the TNTA surface provides the next best agreement with experiment. Since the TNTA, TNTB, MNT, and BNT8 surfaces contain the same repulsive contribution, the differences in the calculated σ_J values are solely due to the different sets of dispersion coefficients. The effect of the dispersion coefficients on the anisotropy of the potentials can be seen by comparing the values of $\Delta\sigma$ and ΔR_V in Table III.

Although the calculated values for $\sigma_{\theta,2}$ follow similar trends as σ_J, the TNTA surface is now doing a much better job, agreeing with the low temperature data and falling just outside of the upper bound of the experimental uncertainty at 400 K. The comparison of the experimental with the predicted temperature dependence of $\sigma_{\theta,2}$ favors the BNT8 and MNT surfaces over the TNTA surface. Table V lists the calculated and experimental values for $\sigma_{\theta,2}$ and σ_J.

V. DISCUSSION

The isotropic part of the BTT potential form has proven reliable for the N_2–lighter rare gas atom interactions. We have already noted in the Introduction section the quality of the transport and other data predicted by the BTT surfaces for N_2–He, N_2–Ne, and N_2–Ar interactions. When considering those properties which specifically depend on the anisotropic part, the ability of the TT model to reproduce experiment appears to decrease in going from He and Ne to Ar as the collision partner. For example, in the N_2–He and N_2–Ne systems, the BTT potentials predict room temperature DPR cross sections and field effect data[2,3] while for the N_2–Ar system, the potential overestimates both room temperature DPR cross sections and the NMR cross sections determined by quadrupolar relaxation.[4] It has been shown[4] that for N_2–Ar the BTT is slightly too anisotropic in the region near σ (that is, $\Delta\sigma$ is too large), while the isotropic part is reasonably good in predicting all those experimental data that are determined in large part by the isotropic part of the potential. The BNT8 surface that we have assembled is the closest analog to the BTT surfaces with the major difference in the derivation of the A and b parameters and the lack of P_4 anisotropy. This surface does not reproduce the experimental B_{12} values but does predict diffusion and viscosity cross sections in agreement with the available experiment. It also overestimates both sets of NMR cross sections. It is not clear whether the fault of this surface is due to the Born–Mayer parameters or the dispersion coefficients. In comparing the A and b parameters determined by the site-to-site charge density overlap combining rule[32] for each orientation (in Table I), the magnitude of A increases in going from N_2–He to N_2–Kr and then for N_2–Xe, decreases to values similar to N_2–Ne for $A_\parallel$ and N_2–Ar for $A_\perp$. The b values generally decrease with increasing mass of the noble gas collision partner with the values for N_2–Ar and N_2–Kr nearly identical. Since the charge distribution data was only available for distances of 3–5 bohr, extrapolated values, assuming an exponential dependence on the distance were used to determine values for the N_2–noble gas interactions.[32] This can lead to

errors in the estimates for the larger distances involved in the N_2–heavy atom interactions. The quality of the exponential form depends on the correlation parameters K and γ used in the power-law type description of the mixed interaction potential energy,[32]

$$V(90°)_{A,BC}=K_{AB}^{(90°)}\left[\frac{S_{AB}^{(90°)}}{R^2}\right]^{\gamma_{AB}^{(90°)}}+K_{BC}^{(90°)}\left[\frac{S_{BC}^{(90°)}}{R^2}\right]^{\gamma_{BC}^{(90°)}}$$

to be independent of the separation of the atoms. The use of the combining rules for K_{AB} and γ_{AB} may be the greatest weakness. Indeed in Table I where the Nyeland–Toennies values can be compared with BTT values, discrepancies of up to about 50% in A and about 4% in b are found.

Of the Tang–Toennies type surfaces, the TNTA surface best reproduces B_{12}, diffusion, viscosity and NMR cross section data. The *ab initio* dispersion coefficients used in this surface were calculated by Thakkar *et al.*[34] and combine the many-body perturbation theory (MBPT) method formulated by Wormer and Rijks[61] applied to N_2 and the same method but without the time-dependent coupled Hartree–Fock (TDCHF) exclusion principle violating (EPV) terms[62] for the noble gas atoms. In the TNTB surface, the dispersion coefficients were determined from the same polarizabilities for the Kr atom but new polarizability and moments of N_2 calculated without the EPV terms. Wormer and Hettema found that the exclusion of these terms gave a better description of the H_2O–H_2O and Ar–NH_3 interactions.[62] The exclusion of the EPV terms brings the approach closer to finite-field MBPT except that Hartree–Fock orbitals which are uncoupled to the external field are used.[35] It is this inadequacy in the treatment of the correlation contribution that led Hettema *et al.* to conclude that the DOSD values should be used for $C_6^{(0)}$ and $C_6^{(2)}$ instead of their MBPT values.[35] Although the TNTB surface utilizes a more consistent set of dispersion coefficients, the combination of the Born–Mayer parameters in the TT form yields a PES that is too anisotropic. At present, it is not clear if the inadequacies of the TNTB surface are due to the charge-overlap combining rule, the MBPT method used in the dispersion coefficients or both.

The MNT surface is most similar to the BNT8 surface and provides insufficient agreement with the experimental data considered. This surface is the only one of the Tang–Toennies type surfaces which explicitly contains only contributions of P_0 and P_2 throughout the surface. In the other TT surfaces, the repulsive parameters are limited to describing P_0 and P_2 symmetry while the dispersion coefficients include additional symmetry contributions. It may be argued that the repulsive parts of the TT surfaces used here do not correctly compensate for the increased anisotropy in the attractive tail, assuming, of course, that the repulsive potential energy is sensitive to higher order anisotropies.

The TNTM surface uses a modified description of the radial dependence of the repulsive interactions in the $\theta=0°$ cut. Originally, the polynomial dependence of the exponential was introduced by Aziz to improve the TT model potential's ability to describe the He–He interaction.[38] We have found this functional form sufficiently flexible to allow the desired similar shapes of the $\theta=0°$ and $\theta=90°$ cuts of the surface. As mentioned, this was done to compare the effect of a parallel repulsive wall which would give rise to a (nearly) constant anisotropy for $R<\sigma$. The TNTM surface differs from the TNTA primarily in the description of the parallel configuration where it provides a stronger repulsion which also increases the anisotropy as shown in the ΔR_V values. As it turns out, the TNT surfaces are too anisotropic already, so this modification makes for a worse agreement between the predictions from this surface with these observables which depend in part on the repulsive wall. The agreement with the B_{12} data of the values calculated from the TNTM surface is also expected since the modification does not significantly alter the volume of the potential bowl. The increased anisotropy along the repulsive wall leads to larger σ_J and $\sigma_{\theta,2}$ values in correspondence with the conclusions of Beneventi *et al.*[4]

The impressive agreement of the GR surface with the NMR cross sections seems to imply that the molecular beam data probes the same parts of the surface as the relaxation cross sections. However, the agreement here may be fortuitous since the CO_2–Ar surface by the same author[22] does not reproduce experimental σ_J values.[53] The molecular beam data used in the fit of the Rotzoll surface is most sensitive to the anisotropy in the well depth (the a_parameter) and to a lesser extent, the isotropic parameters R_m, $\bar{\epsilon}$ and the anisotropy in the radial position of the well (the b parameter).[14] On the other hand, in their multiproperty optimization for the N_2–Ar PES, Beneventi *et al.* found the NMR cross sections to depend on the radial anisotropy.[4] The $\sigma_{\theta,2}$ cross section was most sensitive to the P_2 anisotropy of the radial position of the well in the Morse–Morse–spline van der Waals (MMSV) piecewise potential function for N_2–Ar. The σ_J cross section, which involves the complete quantum mechanical concept of angular momentum reorientation, was found to depend on both the anisotropy in R_m and the P_2 anisotropy in the repulsive wall, although in both cases, the cross sections showed no significant dependence on the anisotropy of the well depth. Therefore the NMR cross sections do indeed provide valuable information on the anisotropy of the potential surface that is not directly probed by the scattering data.

Of the *a priori* Tang–Toennies type potentials, the TNTA surface best reproduces all of the experimental data considered. These TNT surfaces provide a convenient means to compare different anisotropies of a particular functional form and the respective effects on the σ_J and $\sigma_{\theta,2}$ cross sections. The results for the NMR cross sections indicate that the anisotropy of the interaction is best described by the Rotzoll potential among the six PES considered here. The TNTA gives a disappointing second best agreement, and the others are much worse. The much larger ΔR_m, $\Delta\sigma$, ΔR_{1000}, and ΔR_{5000} of these potentials (which uniformly predict too large σ_J and $\sigma_{\theta,2}$ cross sections) compared to Rotzoll's (which predicts σ_J and $\sigma_{\theta,2}$ cross sections that are in good agreement with experiment) underscores the great sensitivity of the molecular reorientation cross sections to the radial anisotropy, which agrees with the earlier conclusions of Ref. 4 for the N_2–Ar system. The sensitivity of these cross sections to the anisotropy in the well depth $\Delta\epsilon$ is demonstrated by the very

different results for the MNT and TNTB surfaces which have identical radial anisotropies (same ΔR_m, $\Delta\sigma$, ΔR_{1000}, and ΔR_{5000}) but which differ greatly in $\Delta\epsilon$. This sensitivity of the molecular reorientation cross sections to $\Delta\epsilon$ has not been noted before.

Of the three transport properties considered here, the calculated values for the thermal conductivity coefficient contain the most uncertainty. This is due first to the use of the first order Chapman–Cowling approximation in determining the pure gas cross sections from experiment. For pure Kr, we reproduce the experimental value for λ_{iso} of 9.49 mW/mK. However, for pure N_2 we calculate a value of 25.64 mW/mK compared to the experimental value[26] of 26.03 mW/mK. Efforts to correct this discrepancy within the first order approximation are in progress.[63] Second, the first order approximation is known to contain ~1% uncertainty when applied to the mixtures due to neglect of polarizations terms.[57(b)]

We now examine the characteristics of the NMR cross sections. It has already been established in the N_2–Ar studies of Ref. 4 that both σ_J and $\sigma_{\theta,2}$ are sensitive to the radial anisotropy in the repulsive wall; an increase in the anisotropy increases the likelihood of the noble gas atom to cause a change in the molecular rotational angular momentum of N_2. This again is found in comparing the results for the TNTA and TNTM surfaces. These surfaces have nearly identical attractive parts and differ significantly in their description of the repulsion in the parallel orientation, leading to a higher repulsive anisotropy for the TNTM surface. Furthermore, we have discovered that σ_J and $\sigma_{\theta,2}$ are somewhat sensitive to the anisotropy of the well depth. The MNT and TNTB surfaces differ in the anisotropy of the well depth where the MNT has a value of 71.79 cm^{-1} for $\Delta\epsilon$ while TNTB has a value of 49.59 cm^{-1}. Even though these surfaces have nearly identical radial anisotropies, the values for the NMR cross sections predicted by the MNT surface are larger than those of the TNTB. The combination of these conclusions, that the radial anisotropy and the anisotropy in ϵ both contribute to σ_J and $\sigma_{\theta,2}$ explains why the TNTB surface predicts larger values for these cross sections than does the TNTA.

In their landmark work on the HCl–Ar system, Neilsen and Gordon studied the ability of various versions of a PES to describe a set of experimental data.[31] Their semiclassical treatment permitted a detailed account of the observables and their dependence on the potential surface and the initial conditions such as the initial rotational energy of HCl, initial relative translational energy and the impact parameter. In the investigation of the NMR relaxation times, Neilsen and Gordon concluded that only the magnitude of spin–rotation relaxation time (which is directly related to σ_J) provides a probe of the PES and that measurements at several temperatures would only serve as a check on the precision of the data. For the HCl–Ar system the temperature dependence was found to follow a simple power law

$$T_1(T)=T_1(300)*(T/300)^n,$$

where the relaxation time goes as the classical value[31] of $n=-3/2$ which implies that the cross section depends on temperature as T^{-1}. Experimental investigations of σ_J in our laboratory for about 100 collision pairs have shown that the temperature dependence of the σ_J cross section (and, of course, the relaxation time) over a 200 degree temperature range can be described by the power law

$$\sigma_J(T)=\sigma_J(300)*(T/300)^{m_J}$$

with $m_J<0$ (Ref. 29 and references therein). For many collision pairs which involve the HCl molecule, m_J is found to be approximately -1. However, this is not necessarily the case for the other collision pairs where the value of m_J varies between -0.6 and -1.6. We find that the power law provides an adequate description of the present trajectory results for $\sigma_J(T)$ over a finite temperature range. Figure 8 shows natural log plots of the calculated σ_J values from the TNTA surface and the best linear fit. In the region of experimental interest, i.e., for 200 K$\leqslant T\geqslant$400 K, [$\ln(T/300)=-0.4$ to 0.3] a single factor of $(T/300)^{m_J}$ describes the temperature dependence where m_J is negative but not equal to unity and in fact, we find the value of m_J to depend on the PES used. Table VI lists the values for m_J (obtained from similar fits) for the various N_2–Kr potentials and does show that the temperature dependence of σ_J (or the related relaxation time) is indeed dependent on the characteristics of the PES. Also in Table VI are listed the values of $m_{\theta,2}$ for the temperature dependence of the $\sigma_{\theta,2}$ cross section,

$$\sigma_{\theta,2}(T)=\sigma_{\theta,2}(300)*(T/300)^{m_{\theta,2}}$$

for the same 200 deg range. As in the case of m_J, each surface predicts a different value for $m_{\theta,2}$. By comparing the difference of $m_{\theta,2}$ and m_J for each of the surfaces, it becomes evident that for these surfaces the temperature dependence for $\sigma_{\theta,2}$ and σ_J are not related. This is fortunate for our origi-

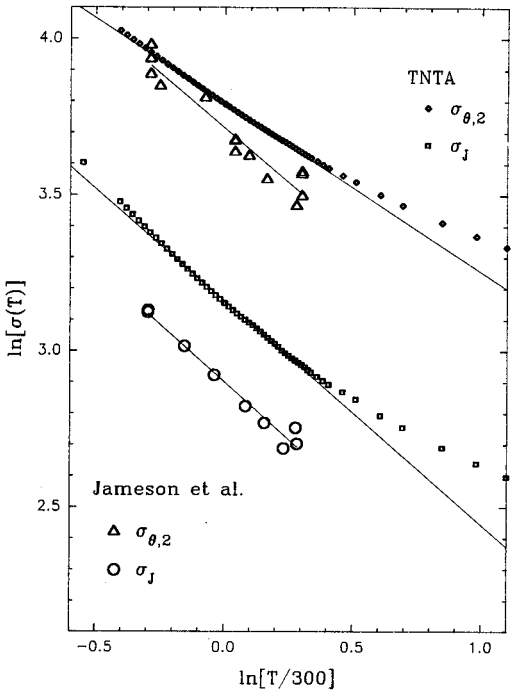

FIG. 8. Power law fits to the temperature dependence of σ_J and $\sigma_{\theta,2}$ from experiment (Refs. 27 and 28) and from the TNTA PES. The straight line fits are made only over the experimental temperature range.

TABLE VI. Results from a power-law fit of the NMR cross sections over a temperature range of 200–400 K.

	GR	TNTA	TNTB	TNTM	MNT	BNT8	Experiment
$\sigma_{\theta,2}$(300 K)	42.11	44.48	49.30	55.31	52.90	55.30	41±2
$m_{\theta,2}$	−0.6205	−0.5455	−0.4684	−0.4957	−0.5170	−0.5190	−0.70±0.06
σ_J(300 K)	19.17	23.67	27.83	29.94	31.60	34.14	18.1±0.5
m_J	−0.8351	−0.7288	−0.6316	−0.6393	−0.7283	−0.7416	−0.74±0.06
$\sigma_{\theta,2}/\sigma_J$	2.197	1.879	1.771	1.847	1.674	1.620	2.3
$m_{\theta,2}-m_J$	0.215	0.183	0.163	0.144	0.211	0.223	0.04
$\sigma_{\theta,2}/\sigma_J$[a]	2.204	1.891	1.771	1.856	1.678	1.702	⋯

[a]Cross section ratios at 300 K from the classical trajectory code.

nal assumption was that the temperature dependencies of the NMR cross sections, not just their magnitudes, are sensitive tests of anisotropic potential surfaces.

Although Neilsen and Gordon did not have experimental values for the quadrupolar relaxation in HCl–Ar, they concluded that both the magnitude and the temperature dependence provide two independent bits of information on the PES. The importance of the temperature dependence for $\sigma_{\theta,2}$ is rationalized by considering the strong energy dependence of the reorientational behavior of the low J states.[31] In our investigations of the NMR quadrupolar relaxation mechanism and the related cross section $\sigma_{\theta,2}$, we have found that the power law also provides a good representation of the temperature dependence for collisions of N_2,[28] NNO,[54] and CD_4 (Ref. 54) with Ar, Kr, Xe, HCl, N_2, NNO, CO, CO_2, CH_4, CF_4, and SF_6. The values for m in these systems is less than zero and varies between −0.6 and −1.0. Likewise, our classical trajectory results show that different descriptions of the N_2–Kr interactions can predict different temperature dependencies.

The ratio of the cross sections, $\sigma_{\theta,2}/\sigma_J$ which has been found to be approximately 2.1 for nearly all N_2–X pairs (X including Ar, Kr, Xe, CO, N_2, CO_2, HCl, CH_4, CF_4, and SF_6) examined experimentally[28] has been a motivation for this work. What we find in Table VI is that for the N_2–Kr system the ratio predicted by different potential surfaces is different, ranging from 1.620 for the BNT8 surface to 2.197 for the GR surface, to be compared with 2.3 from experiment. This again demonstrates that the NMR cross sections are very sensitive to the details of the anisotropy of the potential. It thus appears that taken together, the two NMR cross sections, measured over a range of temperatures, can provide different probes of the PES.

VI. CONCLUSIONS

These classical trajectory results provide the first investigation of collision cross sections from anisotropic potential energy surfaces describing the N_2–Kr interactions. Of the experimental data that we have used to compare the various potential energy surfaces for N_2–Kr, the diffusion coefficients are the least discriminating. All the PES used here gave excellent agreement with experiment, except the TNTM surface. The mixture viscosity is likewise not highly discriminating. Similar results are obtained for the thermal conductivity coefficient showing once again that the TNTA, TNTB, GR, MNT, and BNT8 represent the isotropic part of the surface well enough to reproduce these transport properties. In addition, the TNTA and TNTB surfaces best reproduce the B_{12} experiment, while the other surfaces underestimate the experimental values.

The properties which are known to be sensitive to the anisotropy of the PES are pressure broadening of the depolarized Rayleigh scattering (DPR), gas phase nuclear spin relaxation, and field-effect phenomena (electric and magnetic field effects on transport properties). The temperature dependence of these properties can be used to fit or refine anisotropies of potential energy surfaces. The GR surface predicts the NMR cross sections extremely well with the TNTA giving the next best results. Although the TNTA and TNTB surfaces do not reproduce the NMR cross sections as well as the GR surface does, these TNT surfaces may well be generally better representations of the true surface. The overestimation of the NMR cross sections by the other N_2–Kr surfaces is most likely due to the higher anisotropy in the repulsive wall, embodied by the ΔR_V values listed in Table III. The TNTM surface predicts larger values for the NMR cross sections than does the TNTA or TNTB due to the larger anisotropy in its repulsive wall. This agrees with the results of Beneventi *et al.* who found that an additional $P_2(\cos\theta)$ angle dependence in the repulsive wall gave larger values for $\sigma_{\theta,2}$ for N_2–Ar.[4]

Considering all these data, and the fact that the GR potential was fitted to reproduce molecular beam scattering results, the GR surface gives the best overall agreement with experiment, although it fails in predicting B_{12} values. Since the interaction second virial coefficient depends in such a general way on the PES (i.e., through an integral over the entire surface), this inability to reproduce B_{12} values appears to indicate a basic flaw in the GR surface. The GR surface can be refined to reproduce the pure rotational transitions in the vibrational ground state of the isotopomers of $^{82-86}$Kr–$^{14,15}N_2$ van der Waals complex[64] and improve agreement with the experimental B_{12} values while maintaining the agreement with the diffusion, viscosity, thermal conductivity, and NMR data. This present work suggests the direction of refinement; the isotropic averages R_m and $\bar{\epsilon}$ need to be slightly modified such as to improve the area of the well and the location of the repulsive wall in the isotropic component while maintaining ΔR_m, $\Delta\sigma$, and $\Delta\epsilon$ close to the values for the original Rotzoll potential. The classical trajectory calculations on this refined surface will be reported later.[63] Also, construction of a new N_2–Kr surface is in progress.[65]

In this paper we have reported the first investigation of collision cross sections calculated from anisotropic potential energy surfaces describing the N_2–Kr interactions. We have considered six potential surfaces and found that a simple model potential of a Lennard-Jones form whose parameters have been obtained by fitting to molecular beam scattering data (the Rotzoll potential, used without modification) gives a reasonably good accounting of the two types of NMR relaxation cross sections measured in our laboratory. The characteristics of the anisotropy in the PES that are probed by the NMR cross sections have been considered and it is found that both the radial anisotropy and the anisotropy in ϵ contribute to σ_J and $\sigma_{\theta,2}$. The often-assumed empirical power law dependence of the NMR cross sections on temperature within a 200 deg range is found to be consistent with the results of the classical trajectory calculations of these cross sections, although a more complex temperature dependence would be necessary to describe a much greater temperature range. The description of the temperature dependence of the NMR cross sections by a power law is found to be approximately valid over the typical temperature range (200–400 K) of relaxation measurements in the gas phase, for all of the potentials considered here. The temperature dependence of σ_J and $\sigma_{\theta,2}$ are different for each PES considered here, as should be the case, and differences in the temperature dependence of these cross sections are indeed found experimentally for ten N_2–X pairs.[28] The interpretation of the intriguing approximately $\sigma_{\theta,2}/\sigma_J=2.1$ ratio of these cross sections is still an open question.

ACKNOWLEDGMENTS

This work has been supported by the National Science Foundation (Grant No. CHE92-10790). We are grateful to F. R. W. McCourt for encouraging us in this work and for enlightening discussions. We thank Clement Wong for his help in getting started in the classical trajectory calculations and A. S. Dickinson for permission to use his code. We thank K. T. Tang for helpful discussions about the TT model and Eric Oldfield for the use of an IBM RS/6000 for some of the trajectory calculations.

[1] J. M. Hutson, Annu. Rev. Phys. Chem. **41**, 123 (1990).
[2] L. Beneventi, P. Casavecchia, F. Vecchiocattivi, G. G. Volpi, D. Lemoine, and M. H. Alexander, J. Chem. Phys. **89**, 3505 (1988).
[3] L. Beneventi, P. Casavecchia, G. G. Volpi, C. C. K. Wong, F. R. W. McCourt, G. C. Corey, and D. Lemoine, J. Chem. Phys. **95**, 5827 (1991).
[4] L. Beneventi, P. Casavecchia, G. G. Volpi, C. C. K. Wong, and F. R. W. McCourt, J. Chem. Phys. **98**, 7926 (1993).
[5] C. Lemaire, R. L. Armstrong, and F. R. W. McCourt, J. Chem. Phys. **81**, 5275 (1984).
[6] R. L. Armstrong, M. Bogdan, K. R. Jeffrey, C. Bissonnette, and F. R. W. McCourt, J. Chem. Phys. **99**, 5754 (1993).
[7] R. S. Wagner, R. L. Armstrong, C. Lemaire, and F. R. W. McCourt, J. Chem. Phys. **84**, 1137 (1986).
[8] C. Lemaire and R. L. Armstrong, Can. J. Phys. **63**, 179 (1985).
[9] P. G. Kistemaker and A. E. de Vries, Chem. Phys. **7**, 371 (1975).
[10] S. C. Saxena and R. S. Gambhir, Mol. Phys. **6**, 577 (1963).
[11] D. D. Konowalow and J. O. Hirschfelder, Phys. Fluids **4**, 629 (1961).
[12] C. C. K. Wong, Ph.D. thesis, University of Waterloo, Ontario, Canada, 1991.
[13] W.-K. Liu, F. R. W. McCourt, and A. S. Dickinson, Mol. Phys. **66**, 565 (1989).
[14] R. T Pack, Chem. Phys. Lett. **55**, 197 (1978).
[15] G. Rotzoll, Chem. Phys. Lett. **88**, 179 (1982).
[16] M. S. Bowers, K. T. Tang, and J. P. Toennies, J. Chem. Phys. **88**, 5465 (1988).
[17] K. T. Tang and J. P. Toennies, J. Chem. Phys. **80**, 3726 (1984).
[18] L. Beneventi, P. Casavecchia, and G. G. Volpi, J. Chem. Phys. **85**, 7011 (1986).
[19] C. C. K. Wong, F. R. W. McCourt, and P. Casavecchia, J. Chem. Phys. **93**, 4699 (1990).
[20] F. A. Gianturco, M. Venanzi, and A. S. Dickinson, J. Chem. Phys. **93**, 5552 (1990).
[21] J. Brewer, Technical Report AADD 663448, AFOSR No. 67-2795, Air Force Office of Scientific Research, Arlington, Virginia, 1967.
[22] G. Rotzoll and A. Loebbert, J. Chem. Phys. **71**, 2275 (1979).
[23] R. D. Trengove and P. J. Dunlop, Physica **115A**, 339 (1982).
[24] A. S. M. Wahby, Physica **145C**, 78 (1987).
[25] J. M. Hellemans, J. Kestin, and S. T. Ro, J. Chem. Phys. **57**, 4038 (1972).
[26] R. D. Fleeter, J. Kestin, R. Paul, and W. A. Wakeham, Physica **108A**, 371 (1981).
[27] C. J. Jameson, A. K. Jameson, J. K. Hwang, and N. C. Smith, J. Chem. Phys. **89**, 5642 (1988).
[28] C. J. Jameson, A. K. Jameson, and M. A. ter Horst, J. Chem. Phys. **95**, 5799 (1991).
[29] C. J. Jameson and A. K. Jameson, J. Chem. Phys. **93**, 3237 (1990).
[30] M. Bloom and I. Oppenheim, Adv. Chem. Phys. **12**, 549 (1967).
[31] W. B. Neilsen and R. G. Gordon, J. Chem. Phys. **58**, 4131, 4149 (1973).
[32] C. Nyeland and J. P. Toennies, Chem. Phys. **122**, 337 (1988).
[33] M. S. Bowers and K. T. Tang (private communication, 1991).
[34] A. J. Thakkar, H. Hettema, and P. E. S. Wormer, J. Chem. Phys. **97**, 3252 (1992).
[35] H. Hettema, P. E. S. Wormer, and A. J. Thakkar, Mol. Phys. **80**, 533 (1993).
[36] W. Rijks and P. E. S. Wormer, J. Chem. Phys. **88**, 5704 (1988).
[37] W. J. Meath and A. Kumar, Int. J. Quantum Chem. **S24**, 501 (1990).
[38] R. A. Aziz, A. Krantz, and M. J. Slaman, Z. Phys. D **21**, 251 (1991).
[39] F. R. W. McCourt and L. Bissonnette (private communication, 1992).
[40] F. R. W. McCourt, J. J. M. Beenakker, W. E. Kohler, and I. Kuscer, *Nonequilibrium Phenomena in Polyatomic Gases Part I. The Dilute Gas* (Oxford University, Oxford, 1990), Vol. 1.
[41] F. R. W. McCourt, J. J. M. Beenakker, W. E. Kohler, and I. Kuscer, *Nonequilibrium Phenomena in Polyatomic Gases Part II. Cross Sections, Scattering and Rarefield Gases* (Oxford University, Oxford, 1990), Vol. 2.
[42] S. Chapman and T. G. Cowling, *Mathematical Theory of Nonuniform Gases*, 3rd ed. (Cambridge University, Cambridge, 1970).
[43] C. F. Curtiss, J. Chem. Phys. **75**, 1341 (1981).
[44] C. F. Curtiss and M. W. Tonsager, J. Chem. Phys. **82**, 3795 (1985).
[45] A. S. Dickinson and M. S. Lee, J. Phys. B **18**, 3987 (1985).
[46] W. H. Miller, J. Chem. Phys. **54**, 5386 (1971).
[47] A. S. Dickinson and M. S. Lee, J. Phys. B **19**, 3091 (1986).
[48] H. O'Hara and F. J. Smith, J. Comp. Phys. **5**, 328 (1970).
[49] C. C. K. Wong (private communication, 1992).
[50] E. E. Hanson, C. C. K. Wong, and F. R. W. McCourt, Mol. Phys. **78**, 199 (1993).
[51] C. C. K. Wong, E. E. Hanson, and F. R. W. McCourt, Mol. Phys. **74**, 497 (1991).
[52] C. C. K. Wong, F. R. W. McCourt, and G. C. Corey, Mol. Phys. **78**, 499 (1993).
[53] M. A. ter Horst, C. J. Jameson, J. Sadlej, and M. M. Szczesniak (to be published).
[54] M. A. ter Horst, Ph.D. thesis, University of Illinois at Chicago, 1993.
[55] R. T Pack, J. Chem. Phys. **78**, 7217 (1983).
[56] R. T Pack, Chem. Phys. Lett. **96**, 171 (1983).
[57] (a) F. R. W. McCourt and W.-K. Liu, Faraday Discuss. Chem. Soc. **73**, 241 (1982); (b) J. Chem. Soc. Faraday Trans. 2 **83**, 387 (1987).
[58] R. G. Gordon, J. Chem. Phys. **44**, 228 (1965).
[59] R. G. Gordon, J. Chem. Phys. **44**, 3083 (1966).
[60] C. K. Wong, F. R. W. McCourt, and A. S. Dickinson, Mol. Phys. **66**, 1235 (1989).
[61] P. E. S. Wormer and R. Rijks, Phys. Rev. A **33**, 2928 (1986).
[62] P. E. S. Wormer and H. Hettema, J. Chem. Phys. **97**, 5592 (1992).
[63] F. R. W. McCourt, M. A. ter Horst, and C. J. Jameson J. Chem. Phys. (to be published).
[64] W. Jager, Y. Xu, N. Heineking, and M. C. L. Gerry, J. Chem. Phys. **99**, 7510 (1993).
[65] A. K. Dham and W. J. Meath Chem. Phys. (in press).